Efficient optical pumping of alkaline atoms for evanescent fields at dielectric-vapor interfaces

ELIRAN TALKER,[1] PANKAJ ARORA,[1] YEFIM BARASH,[1] DAVID WILKOWSKI,[2,3,4] AND URIEL LEVY[1,*]

[1]*Department of Applied Physics, The faculty of Science, The Center for Nanoscience and Nanotechnology, The Hebrew University of Jerusalem, Jerusalem, 91904, Israel*
[2]*School of Physical and Mathematical Sciences, Nanyang Technological University, 637371, Singapore*
[3]*Centre for Quantum Technologies, National University of Singapore, 117543, Singapore*
[4]*MajuLab, CNRS-UCA-SU-NUS-NTU International Joint Research Unit, Singapore*
[*]*ulevy@mail.huji.ac.il*

Abstract: We experimentally demonstrate hyperfine optical pumping of rubidium atoms probed by an evanescent electromagnetic field at a dielectric-vapor interface. This light-atom interaction at the nanoscale is investigated using a right angle prism integrated with a vapor cell and excited by evanescent wave under total internal reflection. An efficient hyperfine optical pumping, leading to almost complete suppression of absorption on the probed evanescent signal, is observed when a pump laser beam is sent at normal incidence to the interface. In contrast, when the pump and probe beams are co-propagating in the integrated prism-vapor cell, no clear evidence of optical pumping is observed. The experimental results are supported by a detailed model based on the optical Bloch equation of a four atomic-level structure, which also includes a treatment of transit relaxation and wall collision with relaxation rates that were obtained directly from the thermal velocities of the atoms and the penetration depth of the evanescent wave. The obtained highly efficient optical pumping at the nanoscale is regarded as an important step in the quest for applications such as optical switching, magnetometry, and quantum memory.

1. Introduction

The reflected signal from a dielectric-vapor interface exhibits resonant behavior around the resonance line of the atoms [1–8]. As light is mainly reflected from a thin atomic layer of subwavelength thickness, this method is sensitive to atom-surface interactions [9–15]. Moreover, only atoms flying within this layer will contribute to the reflected signal, whereas atoms with a velocity component normal to the interface rapidly leave the interacting zone. This peculiarity leads to a selective reflection effect both for total internal reflection and normal incidence schemes [2,11,14,16–26]. Light-atoms interactions at the nanoscale with evanescent wave has led to numerous applications such as atomic mirror, magnetometer, optical modulation, optical switching, and other nonlinear effects were demonstrated [16,22,27–34]. In particular, one of the advantages of optical pumping magnetometry is the ability to overcome the deficiency of the random polarization of the atoms. Indeed, one of the ways to increase the polarization of the atoms is by using optical pumping [35]. Therefore, obtaining efficient optical pumping is crucial for achieving high-quality optical pumping magnetometry, as was demonstrated in large, centimeter size cells [36].

Achieving high contrast hyperfine optical pumping with hot vapors is a challenging task due to the Doppler broadening effect. If the pump and probe beams are co/counter-propagating, optical pumping is achieved only for a pre-selected atomic velocity class in resonance with the pump laser beam [33]. Thus, other atomic velocity classes cannot be pumped. If, on the other hand, a cross beam configuration is used, atoms can be pumped regardless of their velocity component along the probe beam. Still, atoms with a velocity component along the pump propagation direction

(perpendicular to the probe), which do not match the pump detuning, will not be pumped. A right-angle prism integrated with a vapor cell has been used to support the evanescent wave under total internal reflection scheme in the vapor [37]. Optical pumping saturation in selective reflection was observed using a single beam experiment [38]. Two-photon evanescent wave spectroscopy in Na atoms has been used by V.G. Bordo et al [40] to explore the transit time broadening and sub-Doppler features. V.G. Bordo et al [7,40] used the cross beam technique in order to determine the collision dynamics of the atoms near the surface, by collecting the fluorescence signal and observing different features for a different group of atoms (i.e. atoms that scattered from the surface and atoms that propagate parallel to the surface).

In this work, we take advantage of the velocity selection process at the nanoscale to demonstrate both theoretically and experimentally efficient hyperfine optical pumping on the reflected evanescent field signal within a cross beam pump-probe scheme. To reveal the optical pumping mechanism in the subwavelength atomic layer, a detailed model based on the optical Bloch equation is developed and compared to our experimental results. The combination of cross beam configuration together with nanoscale confinement of the evanescent wave allows achieving efficient optical pumping, overcoming the limitations posed by the Doppler broadening effect.

2. Theoretical model

Figure 1(a) shows the fine and hyperfine energy level scheme of ^{85}Rb used in the experiment. The $5^2S_{1/2}$ ground state is split into a hyperfine structure with a frequency spacing of $\Delta_{HFS} = 2\pi \cdot 3.035$ GHz. The pump laser is tuned on the $F_g = 2$, $5^2S_{1/2} \rightarrow F_e = 3$, $5^2P_{1/2}$ D_1 transition at 795 nm, whereas the probe laser is scanned over the all $5^2S_{1/2} \rightarrow 5^2P_{3/2}$ D_2 transition at 780 nm. $\delta_1, \delta_2, \delta_3, \delta_4$ are the spacing between the adjacent hyperfine levels as can be seen in Fig. 1(a).

The Doppler frequency broadening in the experiment makes it difficult to resolve the separation of the hyperfine levels. For this reason, the complex level structure of the ^{85}Rb atom is reduced to a four levels scheme as shown in Fig. 1(b). While this simplified level scheme assumption is not sufficient for a control experiment (to be discussed later in the text), it is certainly sufficient to explain the obtained optical pumping between the two hyperfine ground states, noted $|1\rangle$, $|2\rangle$ in our experiment. We keep the same energy splitting as for the ^{85}Rb atom. Levels $|3\rangle$ and $|4\rangle$ are the excited state levels corresponding to D_1 transition and D_2 transition respectively. In the theoretical model, the pump beam is set on the $|1\rangle \rightarrow |3\rangle$ transitions and the probe beam is set between $|1\rangle \rightarrow |4\rangle$ and $|2\rangle \rightarrow |4\rangle$ transitions, respectively. Δ_{pr}, Δ_{pu} are the detunings and Ω_{pr}, Ω_{pu} are the Rabi frequencies of the probe and pump beam respectively. The model also corresponds to our experimental configuration, shown later in Fig. 2.

To study the interaction of the electromagnetic field with atoms, we use the electric dipole interaction operator,

$$V = -\vec{d}_1 \cdot \vec{E}_{pu} - \vec{d}_2 \cdot \vec{E}_{pr} = -\vec{d}_1 \cdot \hat{\varepsilon}_{pu} E_{pu} \cdot e^{i(\omega_{pu} \cdot t + k_{pu} \cdot z)} - \vec{d}_2 \cdot \hat{\varepsilon}_{pr} E_{pr}(z) e^{i(\omega_{pr} \cdot t - k_{pr} \cdot x)} \quad (1)$$

where $\vec{d}_1$, and $\vec{d}_2$ are the dipole matrix element of the D_1, and D_2 transition respectively. E_{pu}, ω_{pu}, k_{pu} and E_{pr}, ω_{pr}, k_{pr} are the amplitude, frequency, and wavenumber of the pump and probe beams, respectively. $\hat{\varepsilon}_{pu} = \hat{x}$ and $\hat{\varepsilon}_{pr} = (\alpha\hat{x} + \beta\hat{z})$ are the electric field polarization of the pump, and probe beams respectively. α and β are constants that depend on the specific conditions of the experiment. The evanescent nature of the probe beam implies that

$$E_{pr}(z) = E_{pr} \cdot \exp(-\kappa_{pr} z) \quad (2)$$

where $\kappa_{pr} = \delta_{pr}^{-1}$, δ_{pr} is the penetration depth, is equal to:

$$\kappa_{pr} = \frac{\omega_{pr}}{c} \sqrt{n_1^2 \sin^2(\theta_i) - 1} \quad (3)$$
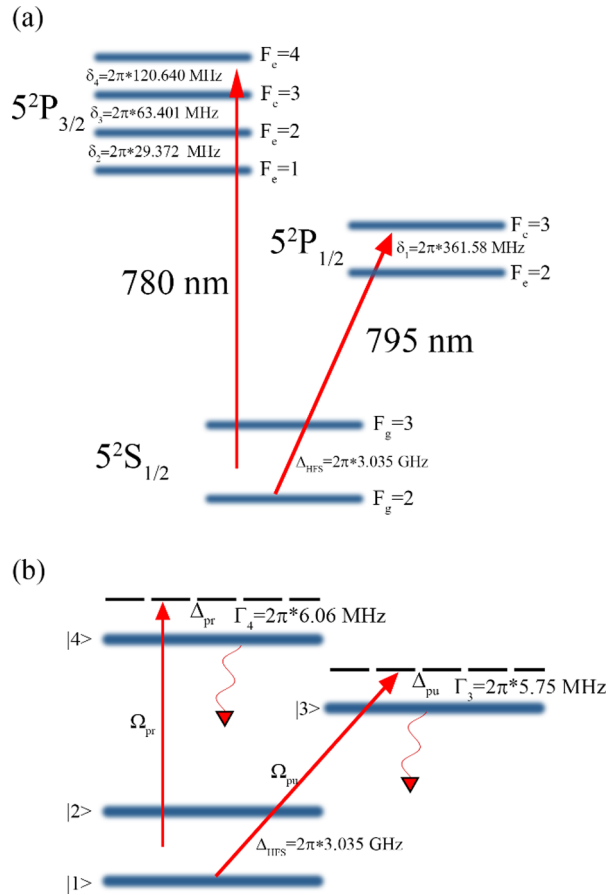
Fig. 1. (a) Fine and hyperfine energy structure of ^{85}Rb considered in the experiment (b) Simplified energy level scheme used for the theoretical model
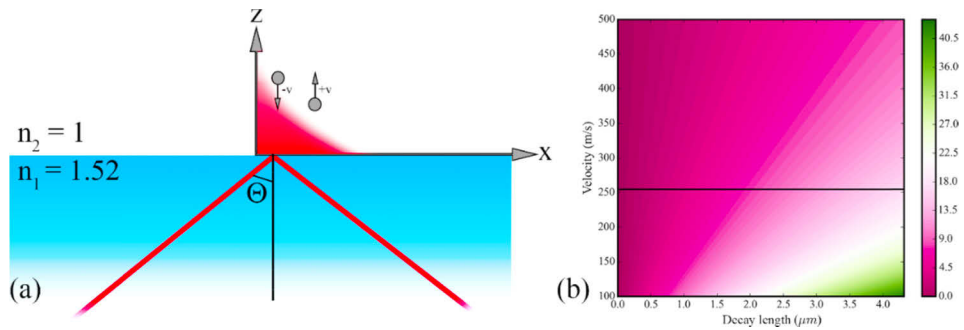

Fig. 2. (a) Schematic of total internal reflection for atoms that moving away (v+) and moving towards (v-) the interface. (b) A color map showing the transit time (in ns) as a function of the decay length and the velocity of the atoms.

here, n_1 is the refractive index of the prism and θ_i is the incidence angle of the probe laser beam, which is slightly larger than the critical angle for total internal reflection.

With these definitions in mind, the interaction operator V can be written as

$$V = -\frac{\hbar}{2}(\Omega_{pu}e^{-i\omega_{pu}t}|1\rangle\langle3| + \Omega_{pr}(z)e^{-i\omega_{pr}t}|1\rangle\langle4| + \Omega_{pr}(z)e^{-i\omega_{pr}t}|2\rangle\langle4| + c.c.) \qquad (4)$$

In matrix form under rotating wave approximation V can be represented as:

$$V = -\frac{\hbar}{2}\begin{pmatrix} 0 & 0 & \Omega_{pu} & \Omega_{pr}(z) \\ 0 & 0 & 0 & \Omega_{pr}(z) \\ \Omega_{pu} & 0 & 0 & 0 \\ \Omega_{pr}(z) & \Omega_{pr}(z) & 0 & 0 \end{pmatrix} \qquad (5)$$

where

$$\Omega_{pr}(z) = -\frac{\vec{d}_2 \cdot \hat{\varepsilon}_{pr}}{\hbar}E_{pr}(z)$$

$$\Omega_{pu} = -\frac{\vec{d}_1 \cdot \hat{\varepsilon}_{pu}}{\hbar}E_{pu}$$

are the Rabi frequencies of the transitions of interest. The evolution of the atomic density operator is governed by the following time-dependent optical Bloch equation:

$$\frac{d\rho}{dt} = -\frac{i}{\hbar}[\mathcal{H}_{tot}(z), \rho] + \mathcal{L}\,\rho - \frac{1}{2}\{\hat{W}(z), \rho\} \qquad (6)$$

here, the Hamiltonian $\mathcal{H}_{tot}$ is the sum of the interaction operator V and the Hamiltonian of the free atom in the rotating frame ($\mathcal{H}_0$), which is equal to

$$\mathcal{H}_0 = \begin{pmatrix} 0 & 0 & 0 & 0 \\ 0 & \Delta_{HFS} & 0 & 0 \\ 0 & 0 & \Delta_{pu} & 0 \\ 0 & 0 & 0 & \Delta_{pr} \end{pmatrix} \qquad (7)$$

$\mathcal{L}$ is the Lindblad relaxation operator,

$$\mathcal{L} = \frac{1}{2}\begin{pmatrix} 2(\Gamma_3\rho_{33} + \Gamma_4\rho_{44}) & 0 & -\Gamma_3\rho_{13} & -\Gamma_4\rho_{14} \\ 0 & 2(\Gamma_3\rho_{33} + \Gamma_4\rho_{44}) & -\Gamma_3\rho_{23} & -\Gamma_4\rho_{24} \\ -\Gamma_3\rho_{31} & -\Gamma_3\rho_{32} & -2\Gamma_3\rho_{33} & -(\Gamma_3 + \Gamma_4)\rho_{34} \\ -\Gamma_4\rho_{41} & -\Gamma_4\rho_{42} & -(\Gamma_3 + \Gamma_4)\rho_{43} & -2\Gamma_4\rho_{44} \end{pmatrix}$$

$$(8)$$

here, Γ_3 and Γ_4 are the natural linewidth for levels $|3\rangle$, and $|4\rangle$ respectively as shown in Fig. 1(b). The diagonal elements of the decay matrix $\mathcal{L}_{ii}$ represent the transfer of population between the atomic levels. The off-diagonal elements represent the decay of the coherence between the levels given by $\mathcal{L}_{ij} = -\frac{\Gamma_i + \Gamma_j}{2} \cdot \rho_{ij}$.

$\hat{W}$ describes the relaxation due to the atom-wall collision which is given by:

$$\hat{W}(z) = \begin{pmatrix} \gamma_c \cdot h(v_z) & 0 & 0 & 0 \\ 0 & \gamma_c \cdot h(v_z) & 0 & 0 \\ 0 & 0 & \gamma_c \cdot h(v_z) & 0 \\ 0 & 0 & 0 & \gamma_c \cdot h(v_z) \end{pmatrix} \tag{9}$$

where

$$\gamma_c = \frac{\bar{v}}{\bar{l}} + \frac{v_z}{z}$$

v_z is the atomic velocity in the direction of the evanescence wave (see Fig. 2(a)), $\bar{l}$ is the mean free path which is $\bar{v}/\Gamma_{SE}$, where $\bar{v}$ is the mean thermal velocity of the rubidium atoms, and $\Gamma_{SE} = \sigma_{SE}\bar{v}_{rel}n_a$ is the spin-exchange rate [39]. Here, σ_{SE} is the spin-exchange cross-section for rubidium, $\bar{v}_{rel} = \left(\frac{8k_BT}{\pi m}\right)^{\frac{1}{2}}$ is the most probable velocity of the rubidium atoms based on the Boltzmann distribution (m is the reduced mass of the two rubidium isotopes), and n_a is the density of the atoms. Our experiment is carried out at the temperature of $70°C$, for which the atom-atom collision rate is negligible compared with the atom-wall collision rate (see Appendix for a detailed explanation) and is therefore neglected. In the relaxation operator $\hat{W}(z)$, $h(v_z)$ is the opposite of the step function, i.e. $h(v_z) = 1$ if $v_z < 0$, and $h(v_z) = 0$ otherwise (i.e. atoms moving away from the interface will not collide with it).

The steady-state regime of the optical Bloch equations is obtained keeping the spatial derivative term of the convective derivative $\frac{d}{dt} = \frac{\partial}{\partial t} + \vec{v} \cdot \vec{\nabla}$. Since the system is supposed to have translational invariance symmetry in the x-y plane, the optical Bloch equations reduce to [40,41]:

$$\frac{d\rho}{dz} = -\frac{i}{\hbar}[\mathcal{H}_{tot}(z), \rho] + \mathcal{L}\,\rho + \frac{1}{2}\{\hat{W}(z), \rho\} \tag{10}$$

Taking into account the Doppler frequency shift,

$$\Delta_{pr} = \Delta_{pr}^0 - k_{pr} \cdot v_x$$

$$\Delta_{pu} = \Delta_{pu}^0 + k_{pu} \cdot v_z$$

here, $\Delta_{pr}^0 = \omega_0^{780} - \omega_{pr}$ and $\Delta_{pr}^0 = \omega_0^{795} - \omega_{pu}$ where $\omega_0^{780} = 2\pi \cdot 384.23\ [THz]$ and $\omega_0^{795} = 2\pi \cdot 377.10\ [THz]$. By applying the boundary conditions $((\rho_{11}(t=0) = \rho_{22}(t=0) = 0.5))$, one can derive an effective optical susceptibility for the probe beam, using the following relation:

$$\chi(\Delta_{pu},\ \Delta_{pr}) \propto \int_{-\infty}^{\infty} dv_z \int_{-\infty}^{\infty} dv_x (\hat{\rho}_{14}(\Delta_{pr}, \Delta_{pu}, v_x, v_z) + \hat{\rho}_{24}(\Delta_{pr}, \Delta_{pu}, v_x, v_z))W(v_x, v_z) \tag{11}$$

where

$$\hat{\rho}_{ij}(\Delta_{pr}, \Delta_{pu}, v_x, v_z) = \int_0^{\infty} \rho_{ij}(\Delta_{pr}, \Delta_{pu}, v_x, v_z,\ z)dz, \tag{12}$$

and $W(v_x, v_z)$ is the bi-dimensional Maxwellian velocity distribution function,

$$W(v_x, v_z) = \frac{1}{2\pi v_T^2} \exp\left(-\frac{v_x^2 + v_z^2}{2v_T^2}\right) \tag{13}$$

where v_x, v_z are the atomic velocity along x and z-direction, respectively, and $v_T = \sqrt{k_BT/m}$ is the thermal velocity of the atomic vapor. k_B, T and m are the Boltzmann constant, the temperature of the gas and the atomic mass, respectively.

The reflectively for TM polarization of the probe beam is defined as:

$$R_p = |r_p|^2$$

where r_p is the reflection coefficient which can be expressed using Fresnel equations as :

$$r_p = \frac{n_1 cos\theta_i - \left(\frac{n_1}{n_2}\right)^2 \sqrt{n_2^2 - n_1^2 sin^2\theta_i}}{n_1 cos\theta_i + \left(\frac{n_1}{n_2}\right)^2 \sqrt{n_2^2 - n_1^2 sin^2\theta_i}} \tag{14}$$

where n_2 is the refractive index of Rubidium vapor,

$$n_2(\Delta_{pu}, \Delta_{pr}) = \sqrt{1 + \chi(\Delta_{pu}, \Delta_{pr})} \tag{15}$$

The penetration depth of the evanescent field, δ_{pr} is given by

$$\delta_{pr} = \frac{1}{k_{pr}} = \left(\frac{\omega_{pr}}{c}\sqrt{n_1^2 sin^2(\theta_i) - n_2^2}\right)^{-1} = \left(\frac{2\pi}{\lambda_0}\sqrt{\left(\frac{n_1}{n_2}\right)^2 sin^2(\theta_i) - 1}\right)^{-1} = \frac{\lambda_0}{2\pi}(n^2 sin^2(\theta_i) - 1)^{-\frac{1}{2}} \tag{16}$$

with $n = n_2/n_1 < 1$. In a typical experiment, with $\lambda_0 = 780$ nm, and θ_i which is slightly detuned from the critical angle for total internal reflection, the penetration depth is about 1 μm.

Throughout this article, the reflectivity simulations were carried out using the above equations.

In order to examine the influence of atoms moving away from the dielectric surface, we start by calculating the time it takes for the atoms to move away from the interface until exiting from the evanescent field. As we can see in Fig. 2(b) even at a v_z of 100 m/s the time it takes for atoms moving in the z-direction to escape from the evanescence field is shorter than the relaxation time (26 ns). Thus, such atoms will not have sufficient time to undergo full optical pumping. (See appendix A for a more elaborate calculation based on rate equations). This brings about the following question: what is the expected efficiency of the optical pumping? To address this question, we calculate (see Fig. 3) the population in each of the ground states using the Optical Bloch equation in the presence of both the pump and the probe beam with intensities of 6 mW and 0.3 mW respectively. As can be seen at velocities of around 100 m/s, the population of the pumped level (ρ_{11}) is around 12% while the population of the other ground state (ρ_{22}) is around ∼85%. Thus, the ratio of ρ_{22}/ρ_{11} in the steady-state regime is about 7, and an efficient optical pumping is expected.
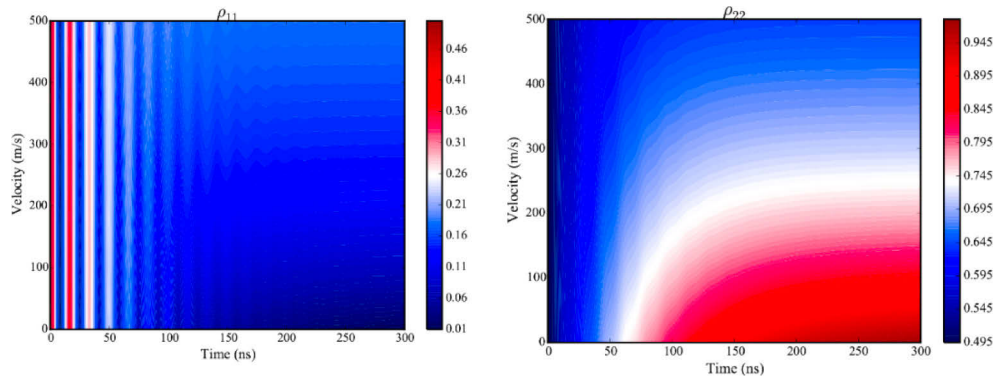

Fig. 3. The population of the two grounds states ρ_{11} (left) and ρ_{22} (right) as a function of velocity and time, assuming a decay length of 1 micron.

3. Experimental results

A schematic drawing of the experimental setup is shown in Fig. 4(a), including a photo of our Rb-vapor cell made of a Pyrex glass tube (tube diameter of 6.5 mm and tube length of 15 mm), terminated one end by a right angle BK-7 prism. The refractive index of the prism is about 1.52 and so the critical angle for total internal reflection is around 42°. A 5 nm thin layer of MgF_2 was evaporated on the BK-7 prism before integrating it to the glass tube to avoid chemical reaction between the BK-7 prism and the Rb vapor. The setup was heated using a homemade oven ($T \sim 70°C$) with a slight temperature gradient to avoid the condensation of rubidium atoms on the surface of the prism.
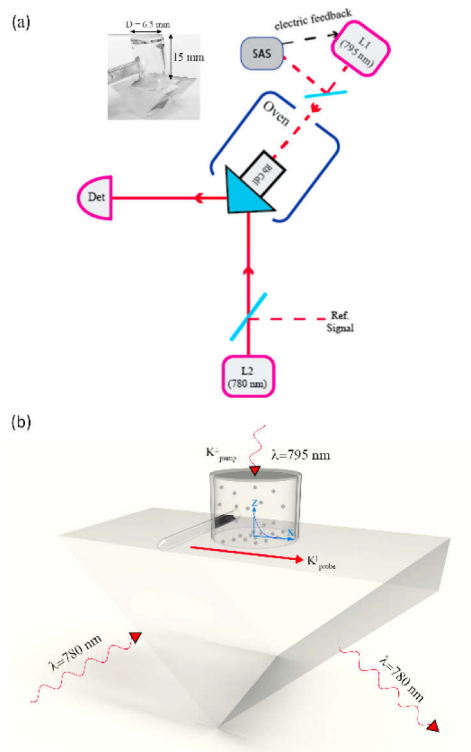

Fig. 4. (a) Experimental Setup used for optical pumping; Inset shows the photograph of Rb-vapor cell which consists of a Pyrex glass tube (tube diameter is 6.5 mm and tube length of 15 mm) and a right angle BK-7 prism (b) Experimental scheme for optical pumping where the wave vectors of the pump and probe beams are perpendicular to each other

In the first experiment, the 795 nm pump laser (L1: TOPTICA Photonics, DL 100) is sent in the vapor cell from the top, and at a normal incidence with respect to the surface of the prism. This laser is frequency locked on the $F_g = 2 \rightarrow F_e = 3$ D_1 line using standard Saturated Absorption Spectroscopy (SAS). The pump beam has a diameter of around 2 mm and an incident power of 6 mW. The optical density is around 1, meaning that a significant fraction of the incident power still makes it to the surface of the prism. The 780 nm probe laser (L2: TOPTICA Photonics, DL pro), with an incident power of 0.3 mW, is sent under total internal reflection conditions (incident angle 43°). Thus, the wave vectors of the pump ($K_{pump}^{\perp}$) and probe ($K_{probe}^{\parallel}$) beams are orthogonal to each other. Beam splitter and mirror are used to tap some of the light from the probe laser. This tapping signal is sent through a 7.5 cm long Rb reference cell (Ref. signal) used for x-axis (frequency axis) calibration purposes and to examine at the same time both the absorption from

the reference cell and the reflection signal from the prism. Figure 4(b) shows schematically the interaction of the evanescent field (blue curve) with the atoms at the dielectric-vapor interface.

Figs. 5(a) and 5(b) show the simulated and experimentally measured reflectivity spectra with (purple curves) and without (blue curves) optical pumping, respectively. When the pump beam is turned off, we observe four absorption lines corresponding to the transition from both ground states ($F_g = 2, 3$) to the F_e manifold for both rubidium isotopes, ^{85}Rb and ^{87}Rb. The lines at around 5.3 GHz and −1.5 GHz, are due to the existence of ^{87}Rb. As we focus on the optical pumping in ^{85}Rb, these lines will be ignored in the forthcoming discussion. Each line has a spectral width of about 600 MHz which is in good agreement with the theoretical linewidth consisting of ~550 MHz Doppler broadening of the D_2 line at T = 70°C, and ~50 MHz transit time broadening due to approximately one-micron penetration depth [6], on top of the natural linewidth of ~6 MHz. When the pump beam is turned on, we can clearly see that the absorption from the ground state $F_g = 2$ nearly vanishes, due to efficient optical pumping of the entire Doppler broadened spectrum. The measured efficiency (solid line) of the optical pumping (i.e. ratio between the two absorption dips) is about 8.5. This agrees very well with the simulated curve (dashed line) at a temperature of 70 °C. The basic explanation for this optical pumping is as follows: the resonant beam, propagating along the z-axis, pumps all the atoms moving in a plane perpendicular to the beam (i.e. the x-y plane) due to negligible Doppler frequency shift. As for the atoms with significant velocity components along the pump propagation direction, here the nanoscale confinement plays at our favor. Those atoms move away from the evanescent beam with a characteristic time of $t = z/v_z$. As a result, such atoms do not have sufficient time to interact with the probe beam propagating along the x-axis.
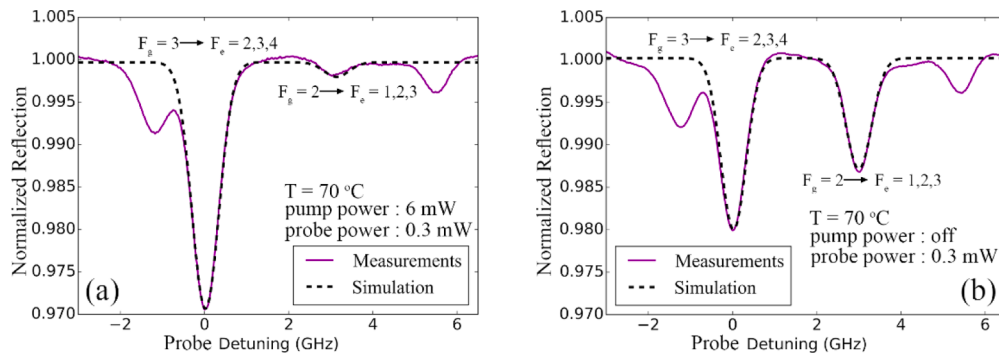

Fig. 5. (a) Simulated and measured reflection for (a) with and (b) without optical pumping respectively as a function of linear probe detuning over the ^{85}Rb $F_g = 3 \rightarrow F_e'$ (zero detuning) and ^{85}Rb $F_g = 2 \rightarrow F_e'$ D_2 resonance line.

To examine the effect of the pump beam intensity on the optical pumping efficiency, we repeated the experiment with different pump beam powers keeping the probe beam power constant (0.3 mW) as shown in Fig. 6(a) (simulation results) and Fig. 6(b) (experimental results). One can clearly see that the decrease in the pump beam power is followed by a reduction in optical pumping efficiency. This result is explained by the fact that by reducing the pump intensity, fewer atoms are excited from the ground state into the excited state. When reducing the pump beam power to about 100 microwatts and below, no optical pumping can be clearly observed.

To further validate our results, we performed a control experiment, where the pump beam (795 nm) with maximum optical power (6 mW) and the probe beam (780 nm: power = 0.3 mW) are co-propagating as shown in Fig. 7(a). To detect only the probe beam, a cascade of two bandpass filters was placed before the detector to reject the 795 nm pump beam. The result obtained from the co-propagating beam experiment is shown in Fig. 7(b). The purple and black
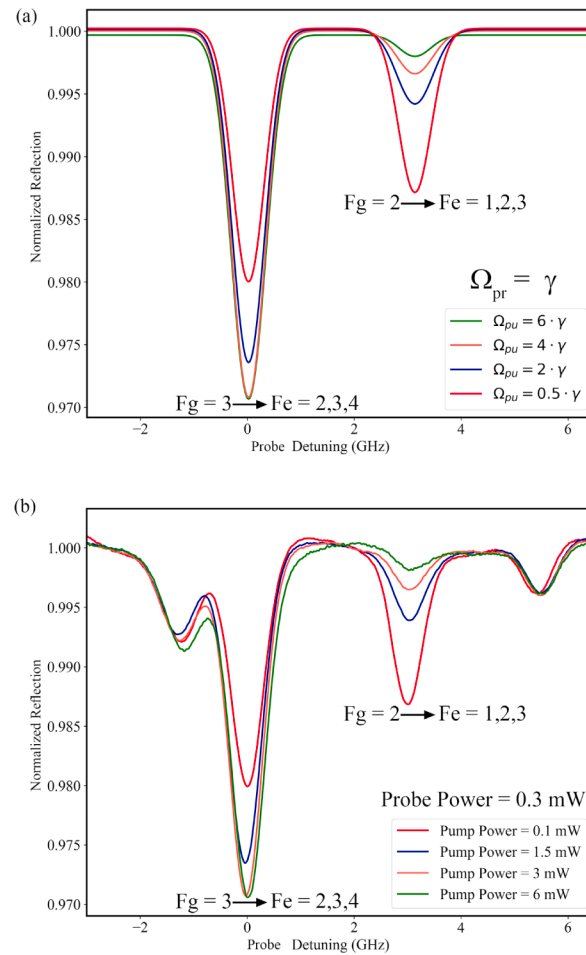
Fig. 6. (a) Simulated and (b) experimental reflectivity measurements for different intensities of the pump beam as a function of linear probe detuning over the ^{85}Rb $F_g = 3 \rightarrow F_e'$ (zero detuning) and ^{85}Rb $F_g = 2 \rightarrow F_e'$ D$_2$ resonance line. The intensity for the probe beam was kept constant (0.3 mW).

lines represent the reflected signal when the pump beam is "off" and "on" respectively. As can be seen, efficient optical pumping is not obtained as compared to the same parameters used in the cross-beam technique (see green line in Fig. 6b). Instead, when the pump beam is on, one can observe (Fig. 7(b), inset) two small peaks within the D_1 absorption lines, which are related to the $F_g = 2 \rightarrow F_e = 2, 3$ transitions. These peaks are the result of a process known as the Velocity Selective Optical Pumping (VSOP) effect [34] (see appendix).
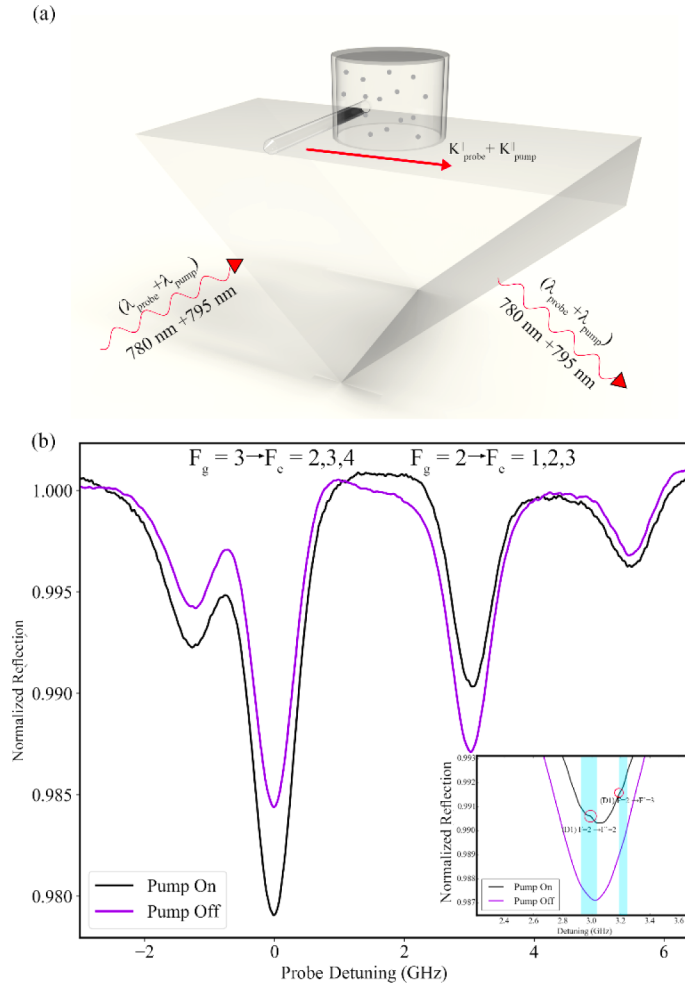

Fig. 7. (a) Experimental setup showing the configuration where the pump and the probe beams are co-propagating in the prism (b) Experimental reflectivity measurements with the pump beam on (black line) and off (purple) as a function of a linear probe detuning over the ^{85}Rb $F_g = 3 \rightarrow F_e'$ (zero detuning) and ^{85}Rb $F_g = 2 \rightarrow F_e'$ D_2 resonance line. The inset shows a zoom in on the $F_g = 2$ transition where the VSOP features are manifested by two small peaks within the resonance dip.

4. Conclusions

In this work, we demonstrated efficient hyperfine optical pumping of an evanescent field at a dielectric-vapor interface using a cross beam pump-probe scheme. The experiment was performed with a Rubidium vapor but could be generalized to any alkaline atoms. A hand-held device was

realized by integrating a right angle prism with a vapor cell. Two pump-probe schemes were presented. In the first configuration, the pump and probe beams were propagating orthogonal to each other, whereas, in the other scheme, the pump and probe beam were co-propagated. Highly efficient optical pumping was achieved only with the first configuration. This is explained by the fact that the pump beam could excite almost all the atoms moving perpendicular to the pump beam due to the negligible Doppler shift. Additionally, atoms with significant velocity component along the pump beam, which cannot be pumped due to Doppler shift, contribute marginally to absorption as they quickly move away of the submicron confined evanescent probe beam. The results were obtained under different pump beam intensities and a decrease in the contrast of optical pumping was noticed with the decrease in the pump beam intensity. To support our experimental observations, we have calculated the expected reflected signal in our system using numerical simulations based on optical Bloch equations. The simulation results were found in good agreement with the observed experimental results. Finally, we believe that the obtained highly efficient optical pumping at nanoscale serves as an important step in the quest for realizing miniaturized quantum devices for diverse applications ranging from optical switching to magnetometry and quantum repeaters.

Appendix

Comparison between wall collision and spin-exchange relaxation rate

As mentioned in the main text, the spin-exchange rate is given by

$$\Gamma_{SE} = \sigma_{SE}\bar{v}_{rel}n_a$$

For ^{85}Rb, the spin-exchange cross-section is equal to [42]

$$\sigma_{SE} = 1.65 \cdot 10^{-14} \ [cm^2],$$

Using the following parameters

$$\bar{v}_{rel}|_{T=70°C} = 29236 \ \left[\frac{cm}{sec}\right]$$

$$n_a|_{T=70°C} = 3.54 \times 10^{11} \ \left[\frac{1}{cm^3}\right]$$

The spin-exchange rate was found to be

$$\Gamma_{SE} = 29236 \cdot 3.54 \times 10^{11} \cdot 1.65 \cdot 10^{-14} \approx 171 \ \left[\frac{1}{sec}\right] \tag{17}$$

For the atom-wall collision, the relaxation rate is given by:

$$\Gamma_{wall} = \frac{v_z}{z} \tag{18}$$

where $v_z|_{T=70°C} = \sqrt{\frac{2 \times k_b \times T}{m_{Rb}}} = 260 \ \left[\frac{m}{s}\right]$ and $z = 10^{-6} \ [m]$. So

$$\Gamma_{wall} = \frac{260}{10^{-6}} \approx 259 \times 10^6 \ \left[\frac{1}{sec}\right] \tag{19}$$

As can be seen, the relaxation rate due to wall collision is an order of magnitude larger than the relaxation rate due to atom collisions ($\Gamma_{wall} \gg \Gamma_{SE}$). Therefore we can neglect the Γ_{SE}.

Optical pumping time

We use the rate equation model in a three-level system (see inset of Fig. 8) to calculate the optical pumping time in the D_1 transition of ^{85}Rb.

$$\frac{dm_1}{dt} = B_{33}\xi(\omega)(m_3 - m_1) + \gamma_{33}m_3 \tag{20}$$

$$\frac{dm_2}{dt} = \gamma_{32}m_3 \tag{21}$$

$$\frac{dm_3}{dt} = -B_{33}\xi(\omega)(m_3 - m_1) - (\gamma_{33} + \gamma_{32})m_3 \tag{22}$$

where m_1, m_2 are the population of the ground states and m_3 is the population of the excited states as can be seen in the inset of Fig. 8. $\xi(\omega)$ is the spectral energy density of a nearly monochromatic beam with an electric field amplitude E. It can be written as

$$\xi(\omega) = \frac{I}{c} \cdot \frac{\frac{\gamma}{2}}{\Delta\omega^2 + \frac{\gamma^2}{4}} \tag{23}$$

γ is the natural linewidth of the transition (for $5^2P_{1/2}$ the natural linewidth is equal to $2\pi \times 5.75$ MHz), $\Delta\omega$ is the laser detuning from resonance, I is the laser intensity and c is the speed of light. B_{33} is the Einstein coefficients for the absorption and stimulated emission of a photon. The excited state decays at a total rate γ consisting of the factorial decay rates into each of the ground states. These fractional decay rates are depending upon the Clebsch-Gordan coefficients, γ_{32} and γ_{33}, according to:

$$\gamma_{32} = \frac{C_{32}^2}{C_{32}^2 + C_{33}^2}\gamma$$

$$\gamma_{33} = \frac{C_{33}^2}{C_{32}^2 + C_{33}^2}\gamma$$

where $C_{32}^2 = \frac{35}{81}$ and $C_{33}^2 = \frac{28}{81}$

As we can see from Fig. 8, the time for observing full optical pumping is around ~0.6 μs which is much slower than the characteristic time that the atoms interact with the evanescent beam.

Velocity selective optical pumping (VSOP)

In our experiment, the pump beam is fixed at the $F_g = 2 \rightarrow F_e = 3$ transition, and due to the Doppler effect it interacts with two groups of atoms, one with zero longitudinal velocity (corresponds to $F_g = 2 \rightarrow F_e = 3$ transition), and the other group with a velocity corresponding to the energy shift $\Delta E(F_e = 2 \rightarrow F_e = 3)$ $\left(v = \frac{2\pi\delta_1}{(2\pi/\lambda_{pu})} = \frac{2\pi \cdot (-361.58\ MHz)}{2\pi/(795\ nm)} = -287\frac{m}{s}\right)$ and as a result, the population in one of the ground state ($F_g = 2$) level is depleted. By examining the probe beam, we observed two small peaks inside the $F_g = 2$ signal due to fewer atoms with the zero longitudinal velocity and also fewer atoms with a velocity that is equal to -287 m/s. This is known as the Velocity Selection Optical Pumping (VSOP) process.
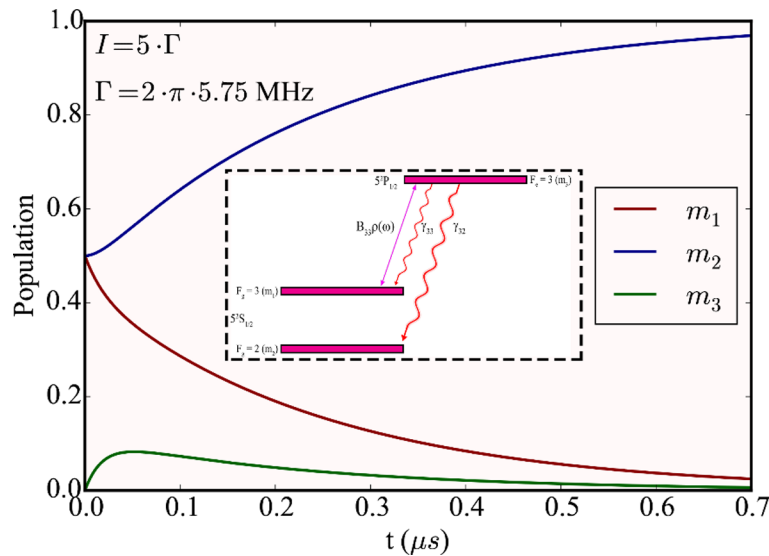
Fig. 8. The population at resonance as a function of time. The inset shows the three-level diagram used for the rate equation model. An intensity of $I = 5\Gamma$ represents the intensity in a typical experiment.

References

1. A. L. J. Burgmans and J. P. Woerdman, "Selective reflection from sodium vapor at low densities," J. Phys. **37**(6), 677–681 (1976).
2. G. Nienhuis, F. Schuller, and M. Ducloy, "Nonlinear selective reflection from an atomic vapor at arbitrary incidence angle," Phys. Rev. A **38**(10), 5197–5205 (1988).
3. T. Matsudo, H. Hori, T. Inoue, H. Iwata, Y. Inoue, and T. Sakurai, "Direct detection of evanescent electromagnetic waves at a planar dielectric surface by laser atomic spectroscopy," Phys. Rev. A **55**(3), 2406–2412 (1997).
4. K. Zhao, Z. Wu, and H. M. Lai, "Optical determination of alkali metal vapor number density in the vicinity (10 - 5 cm) of cell surfaces," J. Opt. Soc. Am. B **18**(12), 1904–1910 (2001).
5. S. T. Ojo, Y. M. Urakami, M. H. Asuo, and T. F. Ujimoto, "Attenuated Total Reflection of the Rubidium D 2 Line in Optically Dense Vapor," J. Phys. Soc. Jpn. **72**(5), 1069–1072 (2003).
6. R. Kondo, S. Tojo, T. Fujimoto, and M. Hasuo, "Shift and broadening in attenuated total reflection spectra of the hyperfine-structure-resolved D2 line of dense rubidium vapor," Phys. Rev. A **73**(6), 062504 (2006).
7. V. G. Bordo, J. Loerke, and H. G. Rubahn, "Two-photon evanescent-volume wave spectroscopy: A new account of gas-solid dynamics in the boundary layer," Phys. Rev. Lett. **86**(8), 1490–1493 (2001).
8. S. Tojo, M. Hasuo, and T. Fujimoto, "Absorption Enhancement of an Electric Quadrupole Transition of Cesium Atoms in an Evanescent Field," Phys. Rev. Lett. **92**(5), 053001 (2004).
9. M. Oria, M. Chevrollier, D. Bloch, M. Fichet, and M. Ducloy, "Spectral observation of surface-induced van der Waals attraction on atomic vapor," Europhys. Lett. **14**(6), 527–532 (1991).
10. A. Laliotis, T. P. De Silans, I. Maurin, M. Ducloy, and D. Bloch, "Casimir-Polder interactions in the presence of thermally excited surface modes," Nat. Commun. **5**(1), 4364 (2014).
11. S. A. Aljunid, E. A. Chan, G. Adamo, M. Ducloy, D. Wilkowski, and N. I. Zheludev, "Atomic Response in the Near-field of Nanostructured Plasmonic Metamaterial," Nano Lett. **16**(5), 3137–3141 (2016).
12. E. A. Chan, S. A. Aljunid, G. Adamo, A. Laliotis, M. Ducloy, and D. Wilkowski, "Tailoring optical metamaterials to tune the atom-surface Casimir-Polder interaction," Sci. Adv. **4**(2), eaao4223 (2018).
13. M. Fichet, G. Dutier, A. Yarovitsky, P. Todorov, I. Hamdi, I. Maurin, S. Saltiel, D. Sarkisyan, M. P. Gorza, D. Bloch, and M. Ducloy, "Exploring the van der Waals atom-surface attraction in the nanometric range," Europhys. Lett. **77**(5), 54001 (2007).
14. V. A. Sautenkov, T. S. Varzhapetyan, H. Li, D. Sarkisyan, and M. O. Scully, "Selective reflection of a laser beam from a dilute rubidium vapor," J. Russ. Laser Res. **31**(3), 270–275 (2010).
15. J. Baudon, G. Dutier, F. Perales, M. Boustimi, and M. Ducloy, "Anisotropic atom-surface interactions in the Casimir-Polder regime," Phys. Rev. A **89**(5), 052514 (2014).
16. A. Sargsyan, A. Papoyan, I. G. Hughes, C. S. Adams, and D. Sarkisyan, "Selective reflection from an Rb layer with a thickness below $\lambda / 12$ and applications," Opt. Lett. **42**(8), 1476–1479 (2017).

17. F. Schuller, O. Gorceix, and M. Ducloy, "Nonlinear selective reflection in cascade three-level atomic systems," Phys. Rev. A **47**(1), 519–528 (1993).

18. G. Nienhuis and F. Schuller, "Selective reflection from a vapor of three-level atoms," Phys. Rev. A **50**(2), 1586–1592 (1994).

19. A. Sargsyan, E. Klinger, Y. Pashayan-Leroy, C. Leroy, A. Papoyan, and D. Sarkisyan, "Selective Reflection from Rb Vapor in Half- and Quarter-Wave Cells : Features and Possible Applications," JETP Lett. **104**(4), 224–230 (2016).

20. J. P. Woerdman and M. F. H. Schuurmans, "Spectral narrowing of selective reflection from sodium vapor," Opt. Commun. **14**(2), 248–251 (1975).

21. A. M. Akulshin, V. L. Velichanskii, A. S. Zibrov, V. V. Nikitin, V. V. Sautenkov, E. K. Yurkin, and N. V. Senkov, "Collisional broadening of intra-Doppler resonances of selective reflection on the D2 line of Cesium," Appl. Phys. Lett. **36**(7), 247–250 (1982).

22. S. Ghezali and A. Taleb, "An evanescent wave atomic mirror," Optoelectron. Adv. Mater., Rapid Commun. **4**(10), 1457–1460 (2010).

23. V. Vuletic, V. A. Sautenkov, C. Zimmermann, and T. W. Hansch, "Measurement of cesium resonance line self-broadening and shift with doppler-free selective reflection spectroscopy," Opt. Commun. **99**(3-4), 185–190 (1993).

24. A. Sargsyan, E. Klinger, G. Hakhumyan, A. Tonoyan, A. Papoyan, C. Leroy, and D. Sarkisyan, "Decoupling of hyperfine structure of Cs D 1 line in strong magnetic field studied by selective reflection from a nano cell," J. Opt. Soc. Am. B **34**(4), 776–784 (2017).

25. A. Laliotis, I. Maurin, M. Fichet, D. Bloch, M. Ducloy, N. Balasanyan, A. Sarkisyan, and D. Sarkisyan, "Selective reflection spectroscopy at the interface between a calcium fluoride window and Cs vapor," Appl. Phys. B: Lasers Opt. **90**(3-4), 415–420 (2008).

26. D. V. Novitsky, "Asymmetric resonance in selective reflection : explanation via Fano-like mechanism," Opt. Lett. **36**(11), 2002–2004 (2011).

27. K. F. Zhao and Z. Wu, "Evanescent wave magnetometer," Appl. Phys. Lett. **89**(26), 261113 (2006).

28. R. Ritter, N. Gruhler, W. Pernice, H. Kübler, T. Pfau, and R. Löw, "Atomic vapor spectroscopy in integrated photonic structures," Appl. Phys. Lett. **107**(4), 041101 (2015).

29. G. Epple, K. S. Kleinbach, T. G. Euser, N. Y. Joly, T. Pfau, P. S. J. Russell, and R. Löw, "Rydberg atoms in hollow-core photonic crystal fibers," Nat. Commun. **5**(1), 4132 (2014).

30. L. Stern, R. Zektzer, N. Mazurski, and U. Levy, "Enhanced light-vapor interactions and all-optical switching in a chip-scale micro-ring resonator coupled with atomic vapor," Laser Photonics Rev. **10**(6), 1016–1022 (2016).

31. V. A. Sautenkov, H. Li, M. A. Gubin, Y. V. Rostovtsev, and M. O. Scully, "Variable Spectral Filter Based on Optically Saturated Selective Reflection," Laser Phys. **21**(1), 153–157 (2011).

32. Y. A. Fofanov and A. A. Rodichkina, "Strong Resonance Reflection of Polarized Light from an Alkali Vapor," Optica Spectroscopy **103**(2), 332–334 (2007).

33. E. Talker, P. Arora, Y. Barash, L. Stern, and U. Levy, "Plasmonic enhanced EIT and velocity selective optical pumping measurements with atomic vapor," ACS Photonics **5**(7), 2609–2616 (2018).

34. L. Stern, M. Grajower, and U. Levy, "Fano resonances and all-optical switching in a resonantly coupled plasmonic-atomic system," Nat. Commun. **5**(1), 4865 (2014).

35. S. J. Seltzer, "Developments in Alkali-Metal Atomic Magnetometry," Princeton University (2008).

36. D. Budker and M. Romalis, "Optical magnetometry," Nat. Phys. **3**(4), 227–234 (2007).

37. P. Arora, E. Talker, N. Mazurski, and U. Levy, "Dispersion engineering with plasmonic nanostructures for enhanced surface plasmon resonance sensing," Sci. Rep. **8**(1), 1–9 (2018).

38. V. Vuletic, V. A. Sautenkov, C. Zimmermann, and T. W. Hansch, "optical pumping saturation effect in selective reflection," Opt. Commun. **108**(1-3), 77–83 (1994).

39. W. Franzen, "Spin relaxation of optically aligned Rubidium vapor," Phys. Rev. **115**(4), 850–856 (1959).

40. V. G. Bordo and H. G. Rubahn, "Two-photon evanescent-wave spectroscopy of alkali-metal atoms," Phys. Rev. A **60**(2), 1538–1548 (1999).

41. V. G. Bordo and H. Rubahn, *Optics and Spectroscopy at Surfaces and Interfaces* (Wiley-VCH, 2005).

42. N. W. Ressler, R. H. Sands, and T. E. Stark, "Measurement of Spin-Exchange Cross Sections for Cs133, Rb87 Rb85, K39, and Na23," Phys. Rev. **184**(1), 102–118 (1969).